

Article

Lignocellulosic-Based/High Density Polyethylene Composites: A Comprehensive Study on Fiber Characteristics and Performance Evaluation

Dimitra Patsiaoura  , Evangelia Tarani  , Dimitrios N. Bikaris  , Eleni Pavlidou  and Konstantinos Chrissafis  ,*

¹ Advanced Material and Devices Laboratory, School of Physics, Aristotle University of Thessaloniki, GR-541 24 Thessaloniki, Greece; dpatsi@physics.auth.gr (D.P.); etarani@physics.auth.gr (E.T.); elpavlid@auth.gr (E.P.)

² Laboratory of Chemistry and Technology of Polymers and Dyes, Department of Chemistry, Aristotle University of Thessaloniki, GR-541 24 Thessaloniki, Greece; dbic@chem.auth.gr

* Correspondence: hrisafis@physics.auth.gr

Abstract: Lignocellulosic-based polymer composites have gained significant interest due to their “green” character as a response to environmental concerns. A diverse array of lignocellulosic fibers is utilized, depending on fiber dimensions, chemical composition, moisture content, and the fiber-matrix interface. The aim of this study is to establish an alternative standardized methodology, aimed at comparatively estimating the performance of polymer composites through the examination of individual plant fibers. The fibers studied are ramie, hemp, flax, and kenaf, and HDPE-based corresponding composites were analyzed for their performance across various fiber-content levels (10, 20, and 30 wt.%). It was found that kenaf showcases the largest average fiber diameter, succeeded by hemp, ramie, and flax. Additionally, ramie and kenaf exhibit elevated levels of crystallinity, suggesting increased cellulose content, with kenaf having the lowest crystallinity index among the fibers compared. Based on Thermogravimetric analysis, ramie displays the lowest moisture content among the examined fibers, followed by hemp, flax, and ultimately kenaf, which is recorded to have the highest moisture content, while, similarly, ramie exhibits the lowest mass loss at the processing temperature of the corresponding composites. Composites containing fibers with smaller diameters and higher crystallinity indexes and lower moisture absorptions, such as ramie and hemp, demonstrate superior thermal stability and exhibit increased Young’s modulus values in their respective composites. However, poor interfacial adhesion affects mechanical performance across all composites. Understanding fiber morphology, inner structure, and thermal stability is important for developing new composite materials and optimizing their selection for various applications.



Citation: Patsiaoura, D.; Tarani, E.; Bikaris, D.N.; Pavlidou, E.; Chrissafis, K. Lignocellulosic-Based/High Density Polyethylene Composites: A Comprehensive Study on Fiber Characteristics and Performance Evaluation. *Appl. Sci.* **2024**, *14*, 3582. <https://doi.org/10.3390/app14093582>

Academic Editor: Giulio Nicola Cerullo

Received: 8 April 2024

Revised: 19 April 2024

Accepted: 19 April 2024

Published: 24 April 2024



Copyright: © 2024 by the authors. Licensee MDPI, Basel, Switzerland. This article is an open access article distributed under the terms and conditions of the Creative Commons Attribution (CC BY) license (<https://creativecommons.org/licenses/by/4.0/>).

Keywords: high-density polyethylene; polymer composites; lignocellulosic fibers; thermal properties; mechanical properties

1. Introduction

Petrochemical-based polymers are known to negatively affect the environment [1], leading to increasing public awareness towards the promotion of “green” products. Hence, environmental rules are continuously legislated by governments [2], while authorities encourage environmental investments in the polymers sector. Among those eco-friendly solutions suggested for the promotion of “green” materials, attention has shifted to polymer composites based on lignocellulosic fibers’ use as reinforcing agents [3–7], which may attribute significant economic benefits, with the ability to play a major role in the automotive and packaging industry, transports, construction, etc. [8–13]. It is well known that the preference for green composites over neat polymers arises from their environmental sustainability, improved performance, cost-effectiveness, and potential for weight

reduction [14–18]. Though, a great deal of technical challenges need to be solved, such as fiber–matrix adhesion, the raise of mechanical performance, poor flammability resistance, and moisture-uptake control [15–18]. Thereafter, there is a demand for the enhancement of the overall performance of natural polymer composites and therefore of the quality of the lignocellulosic fibers used, aiming toward the intensification of their applicability and adaptability in more applications [16].

Natural fibers can lead to composites with low densities and high specific strengths [19]. Furthermore, they possess a great variety of advantages over synthetic fibers, such as that they are low-cost, neutral to CO₂ emissions, biodegradable, have acceptable properties in terms of insulating properties and mechanical performance, are easy to handle and process, and come without health risks. Moreover, they are environmentally friendly, with a low density and high toughness, contributing to waste reduction, increasing energy efficiency, and promoting sustainability [16,20,21]. Though, a series of disadvantages characterize lignocellulosic fibers, such as low strength, high moisture content, limited processing temperatures, low durability, low fire resistance, quality and price variability, and, foremost, incompatibility with hydrophobic polymer matrices [12,16–18].

A great variety of lignocellulosic fibers is available for further use in composite polymers. The quality of natural fibers, and therefore the properties they provide to polymer composites, depend on different factors, reported in detail by Dittenber et al. [21]. In brief, the main factors that affect the fibers' quality when referred to polymer composite manufacture are the species of the plant, the crop location, the local climate, the fibers' ripeness during harvesting, the fiber-extraction methods, the storage conditions, and the age of the fiber [22,23]. Furthermore, the quality of the fibers is greatly affected by the harvesting process, since cell-wall thickness, adherence with the surrounding structure, and the coarseness of fibers vary accordingly to the fiber-production stage in which reaping has been performed. Moreover, Meshram et al. [24] have reported that is quite difficult to define a lignocellulosic fiber's quality.

Nonetheless, although the abovementioned factors affecting fibers' quality are difficult to examine, the composition of natural fibers can be investigated, leading to the estimation of a series of respective polymer composites' properties, such as thermal and mechanical properties [16,25]. Lignocellulosic fibers are mainly composed of three components: cellulose, hemicellulose, and lignin [26]. Cellulose is a non-branched macromolecule which contains chains of different lengths of one–four linked β-d-anhydroglucopyranose units [27]. On the contrary, lignin is a branched structure, serving as the matrix material in which cellulose is embedded, along with hemicellulose [28].

Each component provides to the system totally different properties. More specifically, cellulose has a crystalline structure compared to the other constituents of natural fibers and offers both strength and stiffness to the fibers via linkages (e.g., hydrogen bonds) [18,29–31]. Furthermore, increasing the crystallinity of cellulose leads to decreased elongation, lower water intake and fewer sites available to chemically react with other materials, since tightly packed structures reduce reactive sites' accessibility [32]. On the contrary, hemicellulose has an amorphous structure and among all the fiber's constituents exhibits the greatest sensitivity to thermal effects [18,33,34]. The presence of hemicellulose in lignocellulosic fibers increases the hydrophilic nature of the fibers [18,25], leading to moisture absorption, while it is responsible for biodegradation processes and for reduced thermal stability, leading to thermal degradation at high temperatures [18,29–31]. Lignin, on the other hand, is the most hydrophobic of all the fiber's elements/components, and it likewise exhibits an amorphous structure [35], leading to greater elongation loss and increased thermal stability of natural fibers [18,25].

According to Meshram et al. [24], it is quite difficult to objectively define the concept of quality regarding natural fibers employed in specific applications, leading to a perpetual search of the adequate raw materials for each target utilization. Furthermore, the lack of standardized methods for the determination of the characteristics of natural fibers prevents the suitable

parameter selection from being studied in order to achieve an estimation of certain properties, used for further exploitation in the lignocellulosic-polymer-composites industry.

The aim of this study is to establish an alternative standardized procedure, which will be capable of providing a comparative prediction or/and estimation of the performance assessment of the lignocellulosic-based polymer composites, based on the study of individual plant fibers. It is known that various wet-chemical analytical methods are employed for determining the chemical composition of lignocellulosic fibers, but they are time-consuming and expensive, preventing them from being applied in commercial applications. Furthermore, NIR (Near-Infrared reflectance) Spectroscopy is also a useful tool for extracting chemical information about fibers, but that technique is not commercially friendly [36]. So, this study deals with an alternative standardized method for fibers' analysis based on Scanning Electron Microscopy (SEM), X-ray diffraction (XRD), and Thermogravimetric analysis (TGA), and the way these procedures can optimize the fiber-selection process for various applications as alternative routes toward more commercially friendly methods.

Bast fibers—fibers collected from the stem of the plant—used in the present study are from hemp, kenaf, ramie, and flax. In the literature, their physical and mechanical properties dramatically vary over a large range of values, since inherent variability, as well as the factors mentioned above, lead to an enormous heterogeneity of reported values. Table 1 presents an overview of some of the characteristics of the fibers studied according to a series of studies. These fibers differ in terms of their structure, the number of main building blocks, the content of cellulose and other constituents, water content, etc.

It is worth noting that it is well known that the mechanical performance of plant-fiber-based composites is governed by the efficiency of the stress transfer between the fibers and the polymer matrix through the interface, but the hydrophilic nature of plant fibers, combined with the hydrophobic polymer matrices, end up in ineffective interfacial adhesion [16]. Although, no treatment is applied to natural fibers in present study, since the degree of crystallinity of the fibers can be altered [37], and fibers may be separated into microfibrils, leading to misleading outcomes since the chemical variety involved in the process may affect the fibers in different ways. So, in order to ensure an objective study, without evolving any other factor alteration, natural fibers were used in the current study without any extra pretreatment, no chemical modification, and no coupling agents. So, this study deals with a lignocellulosic-based composite, where fibers and polymer matrices do not exhibit strong interactions; but since the purpose of the article is a comparative study, the materials studied serve that purpose without any interference with the conditions.

Table 1. Overview of reported properties of the four studied lignocellulosic fibers.

Fiber Type	Diameter (μm)	Moisture Content (wt. %)	Cellulose (wt. %)	Hemicellulose (wt. %)	Lignin (wt. %)	Pectin (wt. %)	Waxes (wt. %)	Tensile Strength (MPa)	Young Modulus (GPa)	Elongation (%)	Refs.
kenaf	65–71	6–12	31–72	8–21.5	8–21.5	3–5	0.8	223–930	14.5–53	1.5–2.7	[5,12,16,33,38–40]
hemp	25–500	6.2–12	68–74.4	15–22.4	3.7–10	0.9	0.8	270–900	23.5–90	1–4	[5,16,38–42]
ramie	20–80	7.5–17	68.6–85	13.1–16.7	0.5–0.7	1.9	0.3	220–1000	24.5–128	1.2–4	[18,38–41,43]
flax	12–600	3.9–12	62–72	18.6–20.6	2–5	2.3	1.5–3.3	343–2000	27–103	1.2–3.3	[5,38–43]

2. Materials and Methods

2.1. Materials

HDPE, under the trade name Luminece mPE M5510 EP, was supplied by Total Petrochemicals (Feluy, Belgium). It has a melting temperature of 134 °C and 0.955 g/cm³ density. Ramie, hemp, flax, and kenaf bast fibers (Figure 1) were supplied from Beijing, China. In Figure 1, photographs of the studied fibers are shown, where the white color of the ramie fibers suggests that an additional stage of fiber pretreatment has taken place [44], while the other fibers exhibit yellowish-brownish colors.

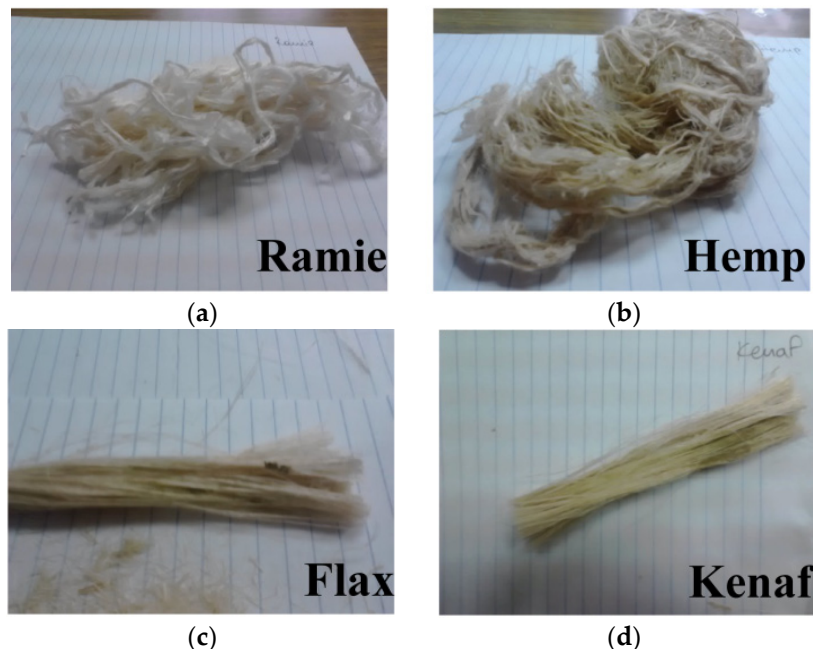


Figure 1. Optical images of fibers studied: (a) ramie; (b) hemp; (c) flax; and (d) kenaf.

2.2. Preparation of Polymer Composites

HDPE and natural fibers were dried at 50 °C under a vacuum for 48 h prior to the melt-mixing, in order to remove the adsorbed moisture, and afterwards they were chopped to 5 mm lengths, and they were physically mixed with HDPE powder. Subsequently, HDPE composites containing 10, 20, and 30 wt.% of each fiber were prepared by melt-mixing in a Haake–Buchler Reomixer (model 600) with roller blades. During the mixing period, the melt temperature and torque were continuously recorded. In each case, 5 min of mixing at 190 °C with a torque speed of 35 rpm was used. The prepared composite materials are coded as HDPE_xx_fiber in the text, where xx corresponds to the mass fraction of each fiber, namely 10, 20, and 30 wt.%, while the word “fiber” corresponds to the specific fiber used in the composites, such as ramie, hemp, flax, and kenaf.

Table 2 presents the composition of the composites prepared, as well as their encoding.

Table 2. Composition of polymer composites and respective encoding.

Sample Name	HDPE wt.%	Fiber wt.%	Fiber Type
HDPE	100	-	-
HDPE_10_ramie	90	10	ramie
HDPE_20_ramie	80	20	
HDPE_30_ramie	70	30	
HDPE_10_hemp	90	10	hemp
HDPE_20_hemp	80	20	
HDPE_30_hemp	70	30	

Table 2. *Cont.*

Sample Name	HDPE wt.%	Fiber wt.%	Fiber Type
HDPE_10_flax	90	10	flax
HDPE_20_flax	80	20	
HDPE_30_flax	70	30	
HDPE_10_kenaf	90	10	kenaf
HDPE_20_kenaf	80	20	
HDPE_30_kenaf	70	30	

2.3. Characterization Techniques

2.3.1. Scanning Electron Microscopy (SEM)

An SEM JEOL JMS-840A-Oxford ISIS 300 model (Jeol Ltd., Akishima, Japan) was employed for the microscopic observation of the fibers' surface characteristics, as well as to perform a qualitative comparison of their surface roughness. It was also employed for the observation of the morphology of the fractured surfaces of the composites. All studied samples were placed on conductive adhesive tapes, sputter-coated with carbon in order to provide good conductivity to the electron beam, and observed under a 20 kV voltage.

2.3.2. X-ray Diffraction (XRD) Analysis

The samples were subjected to X-ray diffraction in a two-cycle Rigaku Ultima+ powder X-ray diffractometer (Rigaku Corporation, Shibuya-Ku, Tokyo, Japan) with a Cu Ka radiation ($\lambda = 0.15418$ nm) operating at 40 kV/30 mA. An XRD analysis of the natural fibers was carried out in a 2θ range of 5–30°. The step size of all measurements was set at 0.05°, while the time per step was set at 3 s. All the samples were measured in similar humidity conditions, and it was assumed that the contribution from the water background was negligible [45].

2.3.3. Thermogravimetric Analysis (TGA)

A Thermogravimetric analysis was performed using a SETARAM SETSYS TG-DTA 16/18, Caluire, France. Samples weighing 4 ± 0.5 mg were placed in alumina pans. An empty pan was used as a reference. Fibers were heated from room temperature up to 1000 °C, while composites were heated from room temperature up to 580 °C. All samples were measured with a 50 mL/min nitrogen gas flow and a 20 °C/min heating rate. For each sample, triplicate runs were performed.

2.3.4. Mechanical Properties

The tensile properties of the polymer composites were measured on an Instron 3344 dynamometer (Norwood, MA, USA), in accordance with ASTM D638 [46], using a crosshead speed of 50 mm/min. Thin films of about 350 ± 25 µm thickness were prepared using an Otto Weber, Type PW 30 hydraulic press connected with an Omron E5AX temperature controller, at a temperature of 190 ± 10 °C. The molds were rapidly cooled by immersing them in water at 20 °C. Dumbbell-shaped specimens were cut in a Wallace cutting press and conditioned at 24 °C and 50–60% relative humidity for 48 h. The values of Young's modulus, tensile stress at break, and elongation at break were determined from stress-strain curves. At least five measurements of tensile mechanical properties were conducted for each sample, while the results were averaged to obtain mean values, as well as standard deviation values.

Izod impact tests were performed in accordance with the ASTM D256 [47] method, using a Tinius Olsen apparatus (Orlando, FL, USA).

3. Results and Discussion

3.1. SEM of Natural Fibers

SEM is an excellent technique for performing a macroscopic analysis of a fiber's morphology by examining the fiber's size and shape, the degree of its surface roughness, and the existence of any surface-lump materials (e.g., wax or other impurities [48]).

The fibers' sizes and shapes constitute the most significant factor related to composite materials, with the effective surface area being inversely dependent on the fibers' dimensions. Thinner fibers expose more effective surface areas than thicker ones, providing greater surface area for contact with the polymer matrix and consequently positively influencing the mechanical properties [49]. Furthermore, the inverse correlation between fibers' diameters and their tensile strength is widely accepted, as a consequence of the fibers' heterogeneous microstructure [50,51]. The main mechanism which is responsible for this correlation lies in the statistical distribution of irregularities throughout the fibers' three spatial dimensions. In the case of small diameters, the density of any defects, flows, or irregularities is smaller in comparison with bigger diameters, with this fact applying both to the surface and to the volume of the fiber. Consequently, thicker fibers tend to be less homogeneous than thinner ones, with a higher density of irregularities, leading to weaker points and stress raisers, capable of leading to premature failure in comparison with thinner fibers.

Moreover, the surface morphology of the fibers plays a vital role in the performance of the final composites. The surface properties of each natural fiber influence the interactions between the polymer matrix and fibers, since wettability is greatly dependent on the morphology of the fibers' surface layer [52]. Roughness on the fiber surface can provide mechanical anchoring to the polymer composite matrix, leading to improved mechanical properties when compared to composites based on fibers with smoother surfaces [49]. The mechanism which leads to that superiority in terms of mechanical properties deals with the increase in specific surface area in the case of grid-like, rough surfaces. In that case, an increased number of hydroxyl groups in the cellulose molecules is exposed, which in turn creates the appropriate conditions for the enhancement of fiber–matrix adhesion through hydrogen bonding [53].

According to the fibers' surface topography, shown in Figure 2, it is evident that all the studied fibers differentiate in terms of all the aforementioned specific surface characteristics, implying the existence of differences on the level of interfacial adhesion that each fiber may exhibit in the matrix, when used as reinforcements. The micrographs of all fibers were taken with $350\times$ [(2a)—ramie, (2b)—hemp, (2c)—flax, (2d)—kenaf], $900\times$ [(2e)—ramie, (2f)—hemp, (2g)—flax, (2h)—kenaf], and $2000\times$ [(2i)—ramie, (2j)—hemp, (2k)—flax, (2l)—kenaf] times magnifications.

In the case of kenaf, its appearance is quite jagged and irregular, since its fibers are mostly composed of connected elementary fibers, forming bundles. Hemp partially exhibits the same behavior, since along with the individual fibers, some bundles are also observed. This may imply some kind of pretreatment to achieve hemp fibers' separation. Hemp fibers, also, exhibit a slightly segmented appearance, with less-grooved surfaces than those of kenaf.

According to SEM microphotographs, flax is the fiber which exhibits the greater lump-material content, since a great number of deposited substances are observed on its surface (Figure 2i). On the other hand, ramie is distinguished for its increased level of smoothness, with a uniform and plain texture, implying a pretreatment process which has led to the removal of any substances on its surface, as has been already mentioned during the fibers' macroscopic examination (Figure 2c).

The obtained SEM images were post-processed with ImageJ 1.50 software, in order to determine the diameters of the fibers, by randomly measuring at least fifty individual fibers of each kind. Although the studied fibers exhibit both irregular shapes and variable dimensions, an assumption is made for reasons of simplification, considering all fibers as cylinders with circular cross sections. The results of the respective measurements are

exhibited in Table 3. It is obvious that the greater mean value of fiber diameter is exhibited by kenaf, following hemp, then ramie, and lastly, flax.

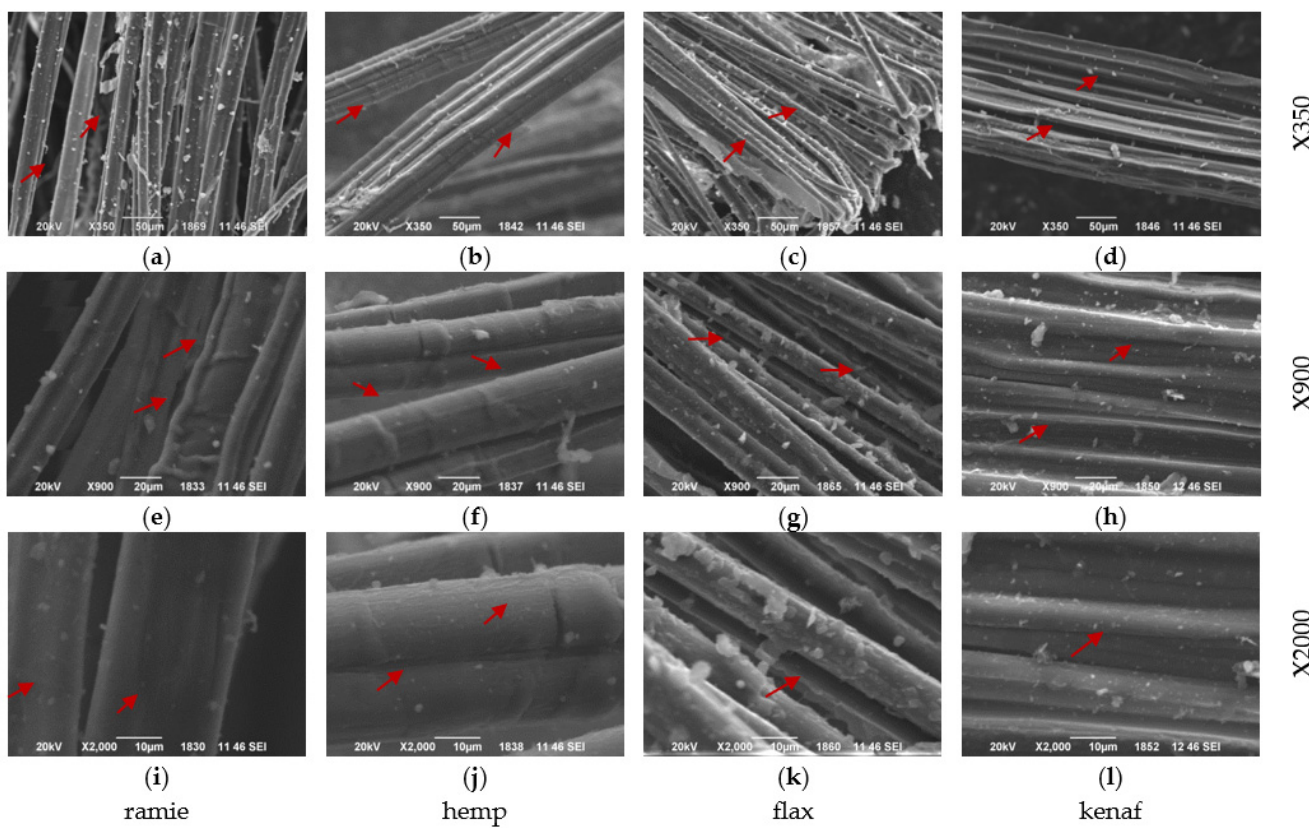


Figure 2. SEM microphotographs of fibers at different magnifications: (a) ramie $\times 350$; (e) ramie $\times 900$; (i) ramie $\times 2000$; (b) hemp $\times 350$; (f) hemp $\times 900$; (j) hemp $\times 2000$; (c) flax $\times 350$; (g) flax $\times 900$; (k) flax $\times 2000$; (d) kenaf $\times 350$; (h) kenaf $\times 900$; and (l) kenaf $\times 2000$. Red arrows highlight specific areas of interest in terms of the fibers' sizes, shapes, surface roughness, and surface-lump materials.

Table 3. Diameters of natural fibers.

Sample	Average Diameter (μm)
Ramie	21.7 ± 7.0
Hemp	24.2 ± 11.1
Flax	14.2 ± 6.5
Kenaf	44.9 ± 14.7

The great differentiation between kenaf and flax, which are the fibers exhibiting the greater and the lower diameter values, is more than obvious in Figure 3, where both SEM micrographs have been obtained under the same magnification of $2700\times$.

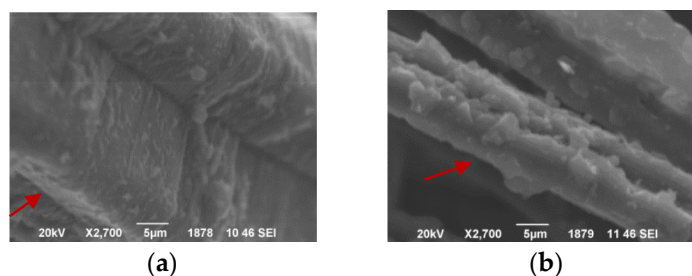


Figure 3. SEM images of (a) kenaf and (b) flax under the same magnification of $2700\times$.

It is of great importance that kenaf and hemp are characterized by the presence of both individual fibers and formed bundles, explaining the corresponding greater values of the standard deviation of the mean fiber diameters. The co-existence of attached and individual fibers is clearly observed in Figure 4.

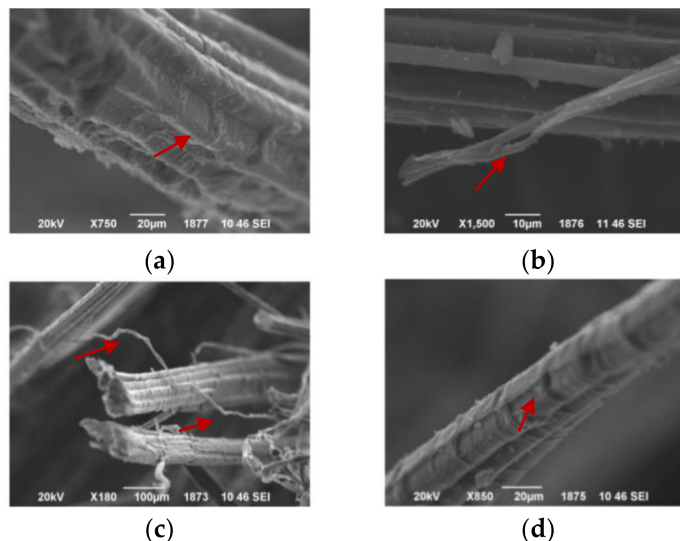


Figure 4. SEM images of (a,b) kenaf and (c,d) hemp, where both individual fibers and bundles are observed.

So, the overall conclusion concerning the studied natural fibers by means of SEM is summarized in the following sentences.

- The roughness of the fibers follows the trend “kenaf” > “flax” > “hemp” > “ramie”;
- The amount of surface impurities on the fibers follows the trend “flax” > “kenaf” > “hemp” > “ramie”;
- Fiber diameter follows the trend “kenaf” > “hemp” > “ramie” > “flax”.

3.2. XRD of Natural Fibers

The XRD measurements of natural fibers were performed in order to estimate the fibers’ crystalline index. All XRD diffractograms were subjected to baseline-correction, and subsequently to peak separation using a Gaussian deconvolution process. The curve-fitting was set, assuming a broad band as the amorphous contribution.

The crystallinity index (Cr.I.) of the fibers is calculated by Equation (1), according to Hermans et al. [54].

$$\text{Cr.I.} = \frac{A_{\text{cryst}}}{A_{\text{total}}} \quad (1)$$

where Cr.I. stands for the crystalline index, A_{cryst} corresponds to the sum of the bands’ areas assigned to crystalline contributions, and A_{total} stands for the total area of the diffractograms.

XRD is a prominent method for the indirect determination of the crystallinity of natural fibers, or, to be more specific, for the ascertainment of the fraction of crystalline cellulose within the entire natural fiber’s content. It is of great importance to mention that among fiber components, hemicellulose and lignin are non-crystalline [55], while only cellulose is crystalline. Consequently, a fiber’s crystallinity refers henceforth to the mass fraction of crystalline cellulose within the fiber.

The Cr.I. is used to describe the relative amount of crystalline material in lignocellulosic fibers. Its calculation is necessary, since cellulosic content is greatly linked to respective mechanical performance. In particular, the fibers’ stiffness rises and their flexibility is decreased by increasing the ratio of crystalline to amorphous material percentages [56].

The X-ray-diffractometry profiles of the studied natural fibers are shown in Figure 5. A series of peaks is observed, which are displayed in Table 4, with their intensities and

their widths varying, as shown in Figure 5. The main contributors to the observable diffraction pattern are three peaks with (1̄10), (110), and (200) Miller indices, with the first two peaks being overlapped. Those peaks are observed from the lowest angle in the aforementioned order. Furthermore, the contribution of the diffraction peak with a (102) Miller reflection is obvious, although seen as a shoulder due to extensive overlapping with the (200) diffraction peak. The (102) diffraction peak, which is scarcely reported, is detected on randomly oriented powder samples of I_β cellulose [57].

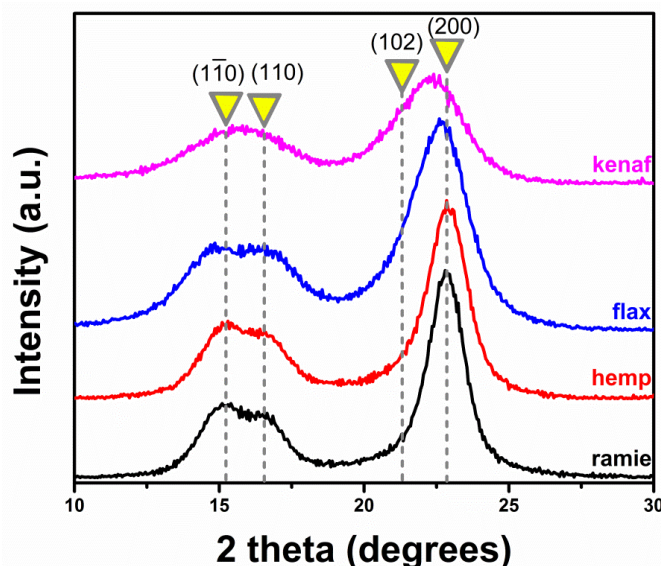


Figure 5. X-ray diffractometry profiles of studied fibers along with their corresponding Miller reflections.

Table 4. The 2θ diffraction peaks of lignocellulosic fibers.

Sample	2θ(°) of 1̄10	2θ(°) of 110	2θ(°) of Amorphous	2θ(°) of 102	2θ(°) of 200
ramie	15.1	16.7	19.2	21.7	22.9
hemp	15.1	16.7	19.4	21.6	22.9
flax	14.5	16.6	19.2	21.7	22.8
kenaf	15.0	16.5	19.2	21.0	22.8

There are various methods which may be implemented for the calculation of cellulose crystallinity. The Segal peak height method [58] is the most common method, though it has been proved to poorly achieve a reliable calculation of crystalline contribution, leading to great errors [59,60]. According to Terinte et al. [61], the peak-fitting method is consistent enough. Consequently, peak deconvolution was used for the thorough examination of natural fibers' diffraction bands and the establishment of both the crystalline and amorphous phases. The diffractograms are shown in Figure 6, and they are deconvoluted with Gaussian-profiled peaks, while a wide Gaussian peak is set between the cellulose (200) diffraction peak and the (1̄10) and (110) diffraction peaks, assigned to the amorphous contribution [62].

After the deconvolution of XRD patterns and the calculation of the crystallinity index of the fibers according to Equation (1), a comparison was performed and tabulated in Table 5, where it becomes obvious that ramie and hemp exhibit greater amounts of crystallinity, and therefore greater amounts of cellulose, while the crystallinity index of flax is decreased compared to the aforementioned fibers, and kenaf has the lowest crystallinity index when compared to the rest of the fibers.

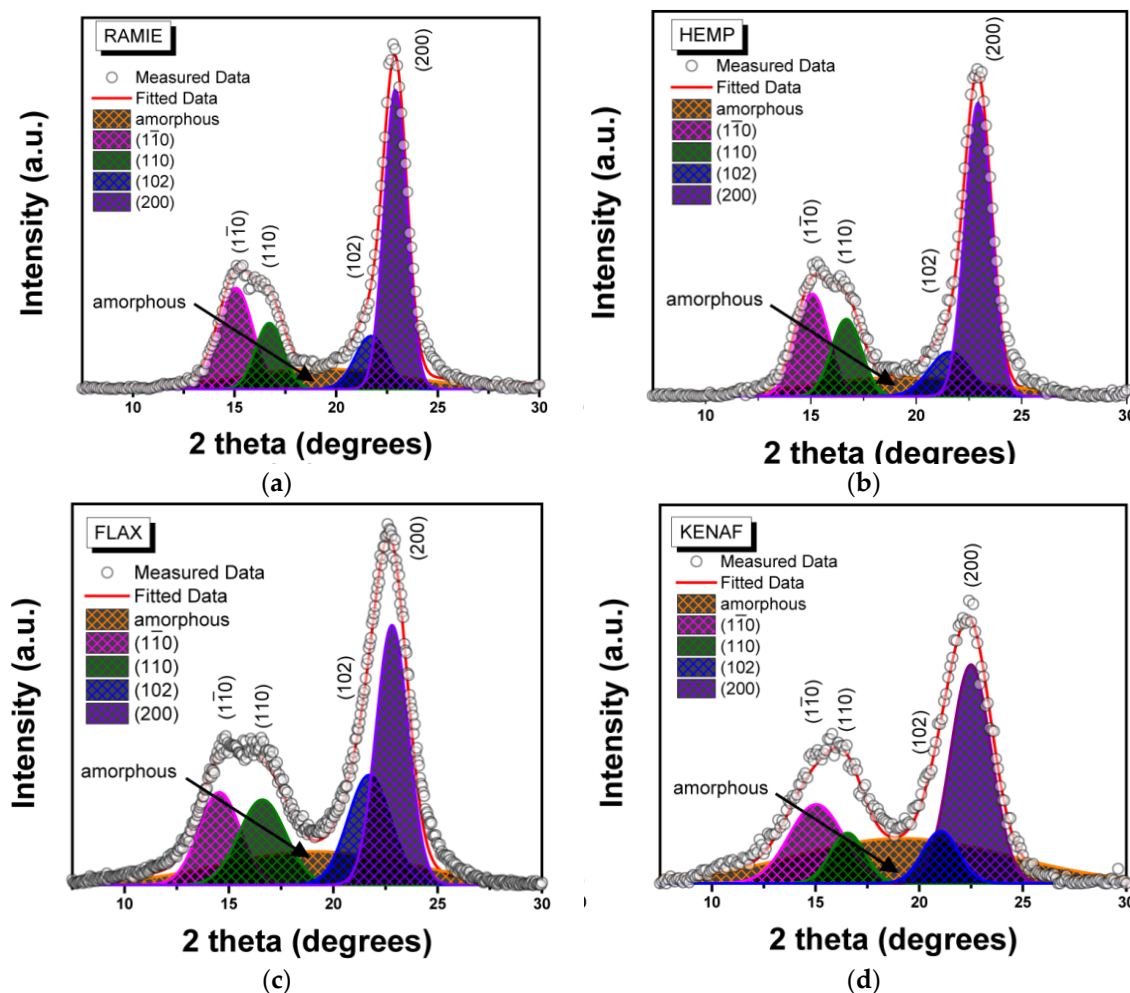


Figure 6. Deconvolution of XRD profiles of (a) ramie, (b) hemp, (c) flax, and (d) kenaf, including the identification of both crystalline and amorphous phases.

Table 5. Crystallinity indexes of natural fibers.

Sample	Cr.I. (%)
ramie	81
hemp	80
flax	77
kenaf	63

3.3. TGA of Natural Fibers

TGA was employed in order to study the thermal stability and degradation profiles of natural fibers (Figure 7a), as well as the mass loss of fibers (%) at the processing temperature of the composites (Figure 7b). It is obvious that all the fibers have a highly similar weight-loss behavior, justifying the need to determine the distinct contribution of each particular component to the thermal performance/behavior of the natural fibers. So, the degradation curves of the fibers are characterized by three distinctive zones. Zone I corresponds to temperatures lower than 200 °C and is mainly attributed to the moisture loss of the fibers [63–66]. Zone II is the region between 200 °C and 500 °C, and its main characteristic are demonstrated by two peaks; one around 300 °C, which corresponds to hemicellulose and pectin content, and another sharper peak which corresponds to the degradation of

cellulosic content [63,65,67]. At higher temperatures, and over the broad temperature range of Zone III, the thermal degradation of lignin takes place [68].

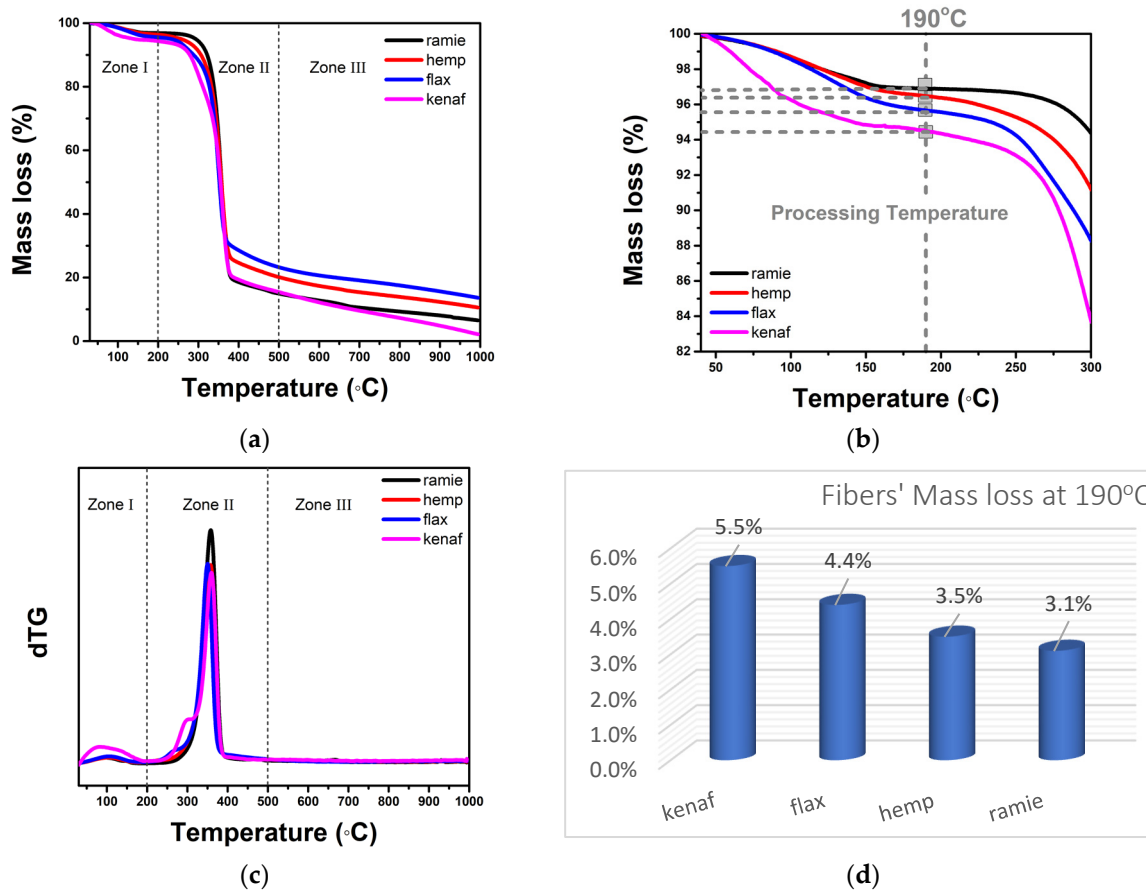


Figure 7. (a) TGA curves of lignocellulosic fibers characterized by three distinctive degradation zones; (b) magnified mass loss of fibers at low temperatures (including processing temperature); (c) dTG curves of all studies fibers; and (d) mass loss of fibers observed at 190 °C.

The processing temperature of composites is considered to be of great importance for the manufacturing of reliable composites. Components of natural fibers start to degrade at relatively low temperatures, where mechanical and thermal properties drastically change [69,70]. The thermal degradation of fibers inside the polymer matrix results in volatile production, leading to porous composites with lower densities and inferior mechanical properties. Therefore, in order to ensure the integrity of the natural composites, it is important to verify that the plant fibers of the composite materials can withstand the heat required during the manufacturing process [71].

The processing temperature of the present study's HDPE_xx_fiber composites must be noticeably well above the melting temperature of HDPE at 134 °C, as already stated, but also low enough to avoid any thermal degradation to the fibers, which may lead to negative effects on the major properties of the composites [70]; this is why composite preparation was performed at 190 °C. In Figure 7b, apart from the mass loss of all the fibers at low temperatures—which correlates to moisture content—the TGA curves of all the studied fibers at the processing temperature of composites are also displayed, where it is more than evident that the fibers' behavior differs radically. It is obvious that at 190 °C, the fiber with the least thermal degradation is ramie, while the fiber with the greatest thermal impact is kenaf, having lost almost 5.5% of its initial mass.

The dTG curves of all studied fibers are exhibited in Figure 7c, where differences for the samples are attributed to content variations. According to the TGA curve of

Figure 7a, mass loss in Zone I is due to the evaporation of absorbed water, while in Zone II there is a shoulder caused by overlapped peaks, mainly caused by hemicellulose, and a sharp peak representing the decomposition of cellulose. Finally, in Zone III, the pyrolysis of lignin is displayed as one long tailing [72]. It is well known that the thermal decomposition of lignin occurs in a wide range of temperatures, since it is a complex process, involving simultaneous reactions, where according to Purnama et al. [73], lignin may start its thermal degradation at around 200 °C to up to 400–450 °C, producing char residue, and may continue with a second thermal-decomposition step above 450 °C, attributed to the formation of oxidized char residue.

In Figure 7d, the fibers' mass loss at the processing temperature is presented, where it can be clearly seen that at 190 °C ramie had lost 3.1% of its initial mass, hemp had lost 3.5% of its mass, flax had lost 4.4%, and kenaf displays the greatest mass loss, which is of 5.5%.

Furthermore, mass loss at low temperatures is correlated to the fibers' moisture content, so according to Figure 7d, the moisture content of fibers follows the trend “ramie” < “hemp” < “flax” < “kenaf”. In general, moisture-absorption capacity is determined by both the content of voids and the non-crystalline regions of the fiber [58]. Moisture uptake is responsible for the swelling of the fiber, and as a consequence for the loss of the dimensional stability (deformation), leading to negative outcomes in terms of physical and mechanical properties. This very reason is the main concern for the utilization of natural fibers in composite applications, since it leads to the deterioration of the overall fiber performance [59].

3.4. Scanning Electron Microscopy (SEM) of Composites

SEM is employed for the evaluation of the extent of interfacial adhesion between fibers and the matrix, while these observations support the results obtained from the mechanical tests. Figure 8 displays the SEM microphotographs of the composites' fractured surfaces.

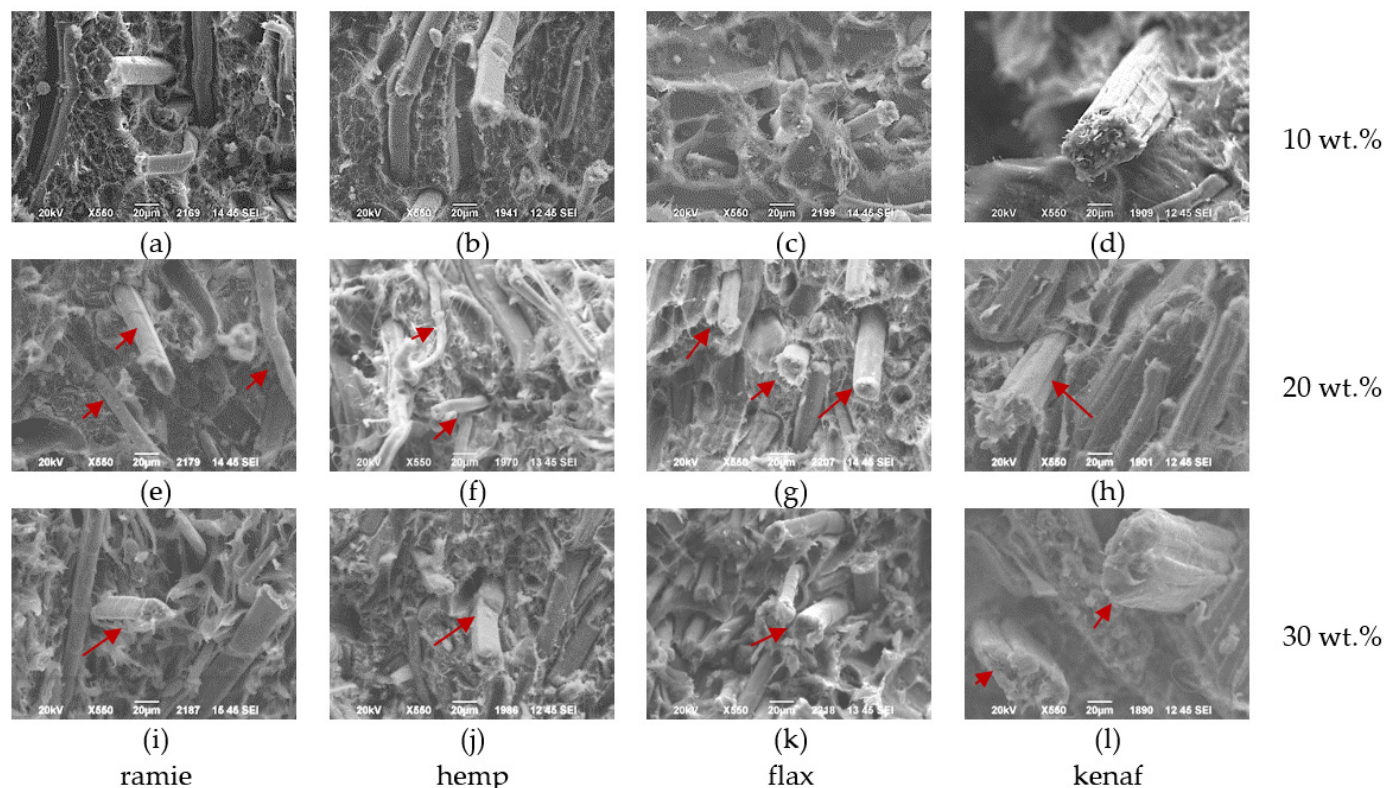


Figure 8. SEM microphotographs of the composites' fractured surfaces: (a,e,i) for ramie; (b,f,j) for hemp; (c,g,k) for flax; and (d,h,l) for kenaf, filled with filler content of 10 wt.%, 20 wt.%, and 30 wt.%, respectively.

As clearly seen in the SEM microphotographs of the composites, pull-out fibers and fiber–matrix debonding can be observed. The fibers have been detached from the polymer matrix during deformation, due to the insufficient interfacial adhesion between the fibers and the polymer matrix. This poor interfacial adhesion between fibers and matrices leads to the low wettability of fibers in the polymer matrix and to the impaired mechanical properties of manufactured composites [12], since no effective load transfer takes place. In general, when interface adhesion is poor, the capabilities of polymer-reinforcing agents cannot be exploited to the full extent.

3.5. Thermogravimetric Analysis of Composites

The thermal stability of lignocellulosic-based polymer composites is crucial; since it helps in predicting the durability and performance of the composite material under certain temperature conditions, it guides the selection of appropriate manufacturing processes and it helps in determining the composites' appropriateness for certain applications. Figure 9 presents the TGA (Figure 9a) and dTG curves (Figure 9b) of HDPE and its hemp-based polymer composites. A gradual shift of curves toward lower temperatures upon fiber-content increase is obvious, and is associated with the fact that incorporated fibers have a distinct contribution to TGA profiles, since they thermally degrade at lower temperatures when compared to HDPE.

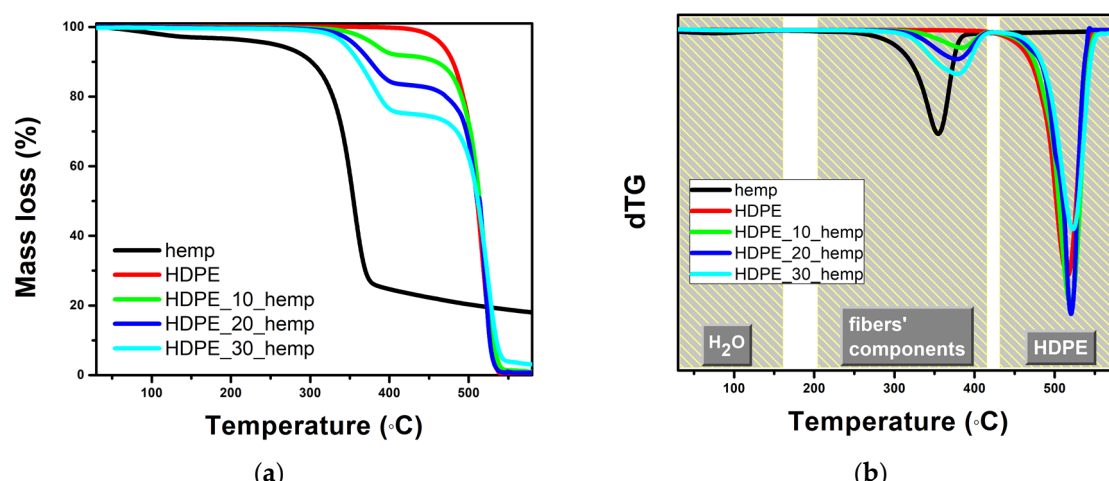


Figure 9. (a) TGA and (b) dTG curves of hemp-based polymer composites filled with varying filler content.

The same behavior occurs in all fiber-based studied composites (Figure 10), where all the TGA curves of studied composites lie in the region between that of HDPE and the corresponding fiber.

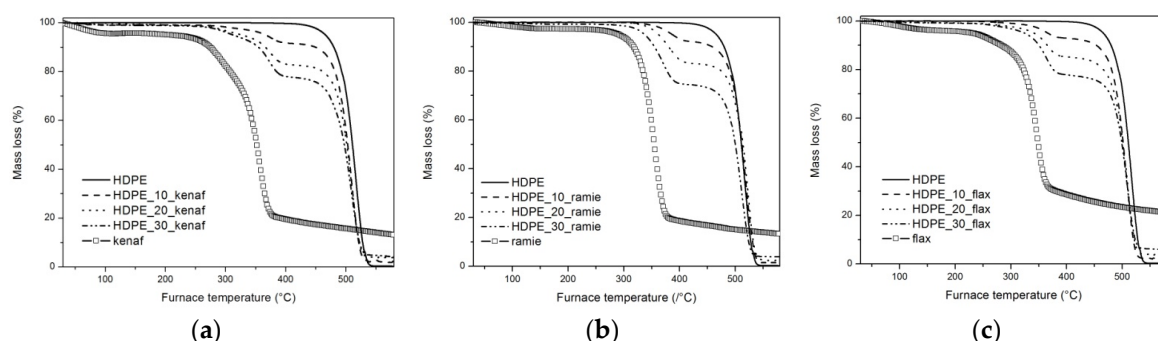


Figure 10. TGA curves of (a) kenaf-based composites, (b) ramie-based composites, and (c) flax-based composites filled with varying filler contents.

In general, the thermal degradation of fiber-based composites takes place in three steps, as seen in Figure 9b. The first one occurs at up to approximately 150 °C, and it is attributed to water loss. Furthermore, a distinct weight-loss curve appears at the region of 150–400 °C, which corresponds to thermal decomposition of the fibers' components, while the third degradation step in the 400–580 °C region is mainly due to the degradation of C-C bonds in the main chain of HDPE [74].

The main thermal parameters of all the composites are presented in Table 6 and in Figure 11. T2% and T5% stand for the temperatures where 2% and 5% of the initial mass has been lost, respectively, while $T_{d,max}$ refers to the decomposition temperature where the maximum mass loss is observed.

Table 6. Thermal properties of the prepared composites.

Sample	T2%	T5%	$T_{d,max}$
HDPE	447	466	516
HDPE_10_kenaf	309	367	509
HDPE_20_kenaf	281	327	509
HDPE_30_kenaf	274	312	509
HDPE_10_hemp	356	382	520
HDPE_20_hemp	337	356	520
HDPE_30_hemp	324	344	523
HDPE_10_ramie	365	388	518
HDPE_20_ramie	345	362	522
HDPE_30_ramie	313	337	511
HDPE_10_flax	337	367	507
HDPE_20_flax	291	342	510
HDPE_30_flax	274	325	508

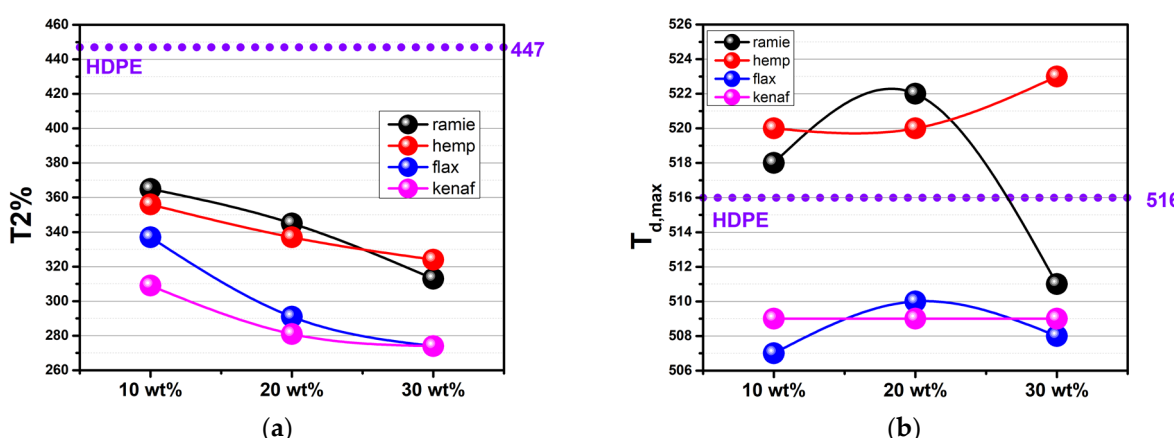


Figure 11. (a) The temperatures corresponding to 2% mass loss (T2%) and (b) the decomposition temperature representing the maximum mass loss ($T_{d,max}$) of all HDPE composites.

It is well known that the thermal performance of each composite depends on the corresponding fiber's chemical composition [16] and mainly on (a) the hemicellulose content of the fiber, since hemicellulose is responsible for mass loss at relatively low temperatures, exhibiting the least thermal resistance among all the fibers' components and (b) on the cellulose content, since it enhances the thermal stability of the composites. Therefore, fibers with a higher hemicellulose content, which means a lower cellulosic content and a lower % cellulose crystallinity, are susceptible to thermal degradation at low temperatures.

As is obvious from Figures 9 and 10, the incorporation of lignocellulosic fibers negatively influences thermal stability of the matrix, since, while the mass loss of HDPE begins

at 415 °C, all fiber-based composites start losing weight almost immediately upon heating, due to the evaporation of water. Therefore, according to Table 6 and Figure 11a, the T2% values of all composites are lower than the corresponding values of HDPE, and thermal stability is decreased upon increasing filler content. Furthermore, the thermal superiority of ramie- and hemp-based composites is obvious in Figure 11a, due to the fact that corresponding fibers exhibit higher crystallinity indexes and less moisture absorption, more crystalline regions, and higher cellulosic contents. Therefore, the T2% values of ramie- and hemp-based composites are higher than the corresponding T2% values of flax-based composites, while the T2% values of kenaf-based composites exhibit the lowest values.

Furthermore, the $T_{d,max}$ values of all composites are presented in Figure 11, where once more it can be observed that ramie- and hemp-based composites improve the corresponding parameter when compared to the rest of the composites, but also when compared to neat HDPE, with the exemption of the HDPE_30_hemp sample, where the $T_{d,max}$ value is significantly reduced, probably due to the poor dispersion of fibers within the polymer matrix, which can create regions of stress concentration and accelerate thermal degradation.

3.6. Mechanical Properties of Composites

The mechanical performance of composites depends on a series of key parameters, such as the (1) particle size, (2) volume fraction, (3) orientation of the filler, (4) mechanical characteristics of both the filler and the matrix, (5) filler–matrix adherence, (6) degree of filler dispersion, etc. [12]

It is well known that the adhesion strength at the interface of composites' components determines the load transfer between them, which is a crucial parameter for composite strength and toughness. On the contrary, Young's modulus is not affected by adhesion quality, because debonding is not observed for small displacements [75]. So, since no treatment is applied to the natural fibers in the present study, it is expected that the strength and toughness of composites will be inferior to the corresponding ones of neat HDPE, while the elastic modulus values of the composites are expected to demonstrate an improved behavior compared to that of the neat polymer. The mechanical properties of HDPE_xx_fiber composites are presented in Table 7 and Figure 12.

Table 7. Mechanical properties of the prepared composites.

Sample	Tensile Stress at Break (MPa)	Elongation at Break (%)	Young's Modulus (MPa)	Impact Strength (J/m)
HDPE	36.1 ± 1.5	716.7 ± 24.8	678 ± 56	577.3
HDPE_10_kenaf	24.8 ± 1.1	2.9 ± 0.3	721 ± 127	96.3
HDPE_20_kenaf	19.9 ± 1.3	1.7 ± 0.1	789 ± 90	84.9
HDPE_30_kenaf	17.5 ± 1.5	1.7 ± 0.2	991 ± 111	75.8
HDPE_10_hemp	20.6 ± 1.7	5.5 ± 0.6	847 ± 87	89.3
HDPE_20_hemp	25.9 ± 2.1	3.6 ± 0.3	1206 ± 105	81.0
HDPE_30_hemp	26.0 ± 1.8	2.7 ± 0.2	1330 ± 101	48.7
HDPE_10_ramie	29.5 ± 1.6	5.4 ± 0.6	1213 ± 95	90.8
HDPE_20_ramie	23.2 ± 1.8	3.6 ± 0.3	1317 ± 121	63.6
HDPE_30_ramie	25.0 ± 1.9	2.5 ± 0.2	1279 ± 173	53.5
HDPE_10_flax	27.0 ± 1.4	5.1 ± 0.5	1128 ± 114	81.6
HDPE_20_flax	27.8 ± 1.2	3.8 ± 0.3	1266 ± 163	70.5
HDPE_30_flax	28.1 ± 2.0	3.4 ± 0.5	1383 ± 135	66.9

Figure 12a displays the Young's modulus of HDPE and its composites. The introduction of different kinds of fibers in HDPE leads to a gradual increase in the elastic modulus in almost every studied composite, which is in all cases higher than that of neat HDPE. More specifically, for 10, 20, and 30 wt.% of ramie fibers, Young's modulus was found to be 79, 94, and 89% higher than that of the neat matrix, with the HDPE_30_ramie being

the only composite that displays a slight decrease compared to its 20 wt.% corresponding composite. A gradual increase in terms of the elastic modulus was observed for 10, 20, and 30 mass% of hemp fibers (23, 78 and 96%) and of flax fibers (66, 87 and 104%). Regarding the kenaf fibers, the same increasing trend is observed in terms of the elastic modulus, too, but to a lower extent, since the corresponding composites were found to be 6, 16, and 46% higher than that of neat HDPE. This is due to the fact that kenaf exhibits the lowest cellulose crystallinity (63%) compared to the rest of the fibers, as shown by the XRD deconvolution method, and also kenaf fibers possess a greater diameter compared to the rest of the fibers, as shown by the SEM microphotographs. However, in all cases, stiffer composites are prepared when compared to the neat HDPE.

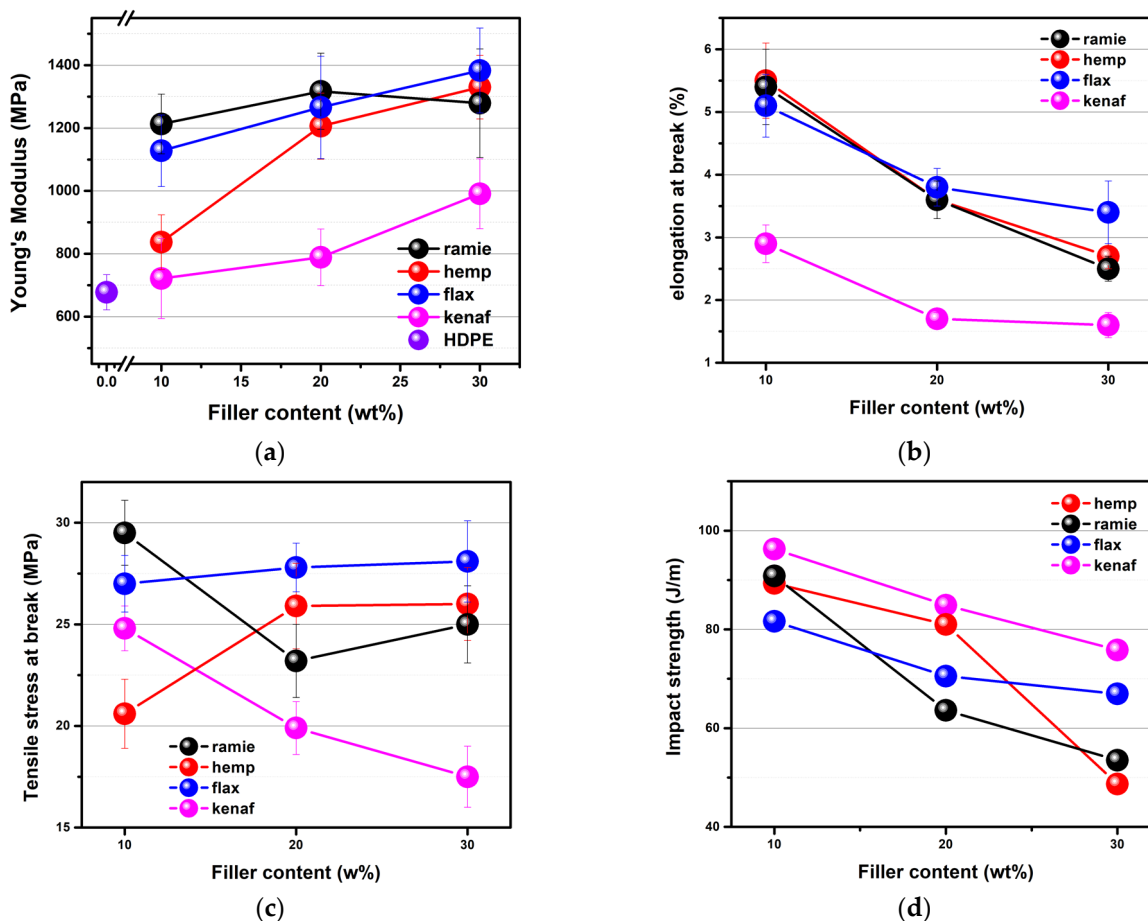


Figure 12. Mechanical properties of the prepared HDPE composites: (a) Young's modulus, (b) elongation at break (%), (c) tensile stress at break (%), and (d) impact strength (J/m).

The elongation at break of all the samples is displayed in Figure 12b, where it is obvious that a premature fracture of all the composites has taken place, since although HDPE's value is $716.7\% \pm 24.8\%$, all the composites' values range from 1.7% to 5.5%. So, the mechanical behavior of the material has been totally altered, since fracturing has taken place without significant plastic deformation or elongation, known as brittle fracturing.

The tensile stress at break of all composites (Figure 12c) is lower than the corresponding stress of neat HDPE due to the microstructure of the composites, since inadequate interfacial bonding is achieved [75], and structural irregularities may have been introduced during processing. More specifically, due to poor matrix–fiber adhesion, as indicated by the SEM microphotographs, the stress transfer at the polymer–fiber interphase is inefficient, while voids and fiber agglomerates promote the premature failure of composites when compared to the neat matrix. However, with the increase in fiber content, there are three different behaviors observed in the studied composites. Hemp-based composites become stronger,

flax-based composites exhibit minute strength alteration, and ramie and kenaf composites become less strong. Generally, parameters affecting the strength of composites are related to filler–matrix interfacial adhesion, filler size, and filler loading, while the interplay between the abovementioned three factors can lead to various trends when referring to the effect of filler loading on the strength of composites [75].

At low-weight percentages of lignocellulosic fibers, the HDPE_10_hemp composite displays a low-tensile stress-at-break value, probably due to the fact that hemp fibers, with diameters of $24.2 \pm 11.1 \mu\text{m}$, probably are not well distributed and form agglomerations, while as the weight percentage of fibers increases, a better distribution of fibers may be achieved, with a more interconnected fiber network, leading to enhanced load-bearing behavior.

Flax-based composites maintain approximately the same strength value upon filler increase, due to a combination of factors including the fibers' diameter, dispersion degree inside the matrix, and fiber–matrix interaction. Fibers' small diameters make a distinct contribution to the formation of a well-interconnected network at all filler contents, while the high impurity contents on the fibers' surface may reinforce fiber–matrix interfacial bonding and a 4.4% mass loss of fibers at processing temperatures, which may have caused the formation of voids in the composite. Furthermore, Svab et al. [76] have proposed that during the evaluation of tensile strength at break, small differences in respective values for low filler contents are related to the small impact of fibers on the matrix due to the small interfacial area, while for higher filler contents, an enlargement of the interfacial area and increased interfacial interactions between the matrix–filler are caused.

On the contrary, kenaf-based composite behavior may be associated with a variety of factors. The weak interfacial interaction of the matrix–fiber, as evidenced by the SEM microphotographs, leads to stress-concentration points or defects, reducing the strength. Furthermore, the elevated moisture content of fibers, as evidenced by TGA, may lead to the formation of big voids during processing, negatively affecting the mechanical properties of respective composites. The relatively low cellulose crystallinity, which is the component conferring strength to the fibers, and the greater diameter among the studied fibers, which has a negative effect on dispersion state, have resulted in composites where the reinforcing agents have difficulty in carrying loads as effectively as the rest of the composites.

Furthermore, ramie-based composites exhibit a different behavior, which is the result of different, and in some cases contradictory, mechanisms. At 10 wt.% of filler, ramie-based composites have a high value of tensile stress at break, because of their high cellulosic content and small fiber diameter, which form an interconnected network of well-dispersed fibers. Furthermore, ramie exhibits low mass loss at the processing temperature, which means that void formation is not intense. However, at 20 wt.% of ramie content, there is a decrease in the tensile stress at break, due to the smooth surface of the fibers, leading to weak adhesion between the matrix and the reinforcing agent. Finally, at 30 wt.% of ramie content, the composite's tensile stress at break increases, probably due to well-dispersed fibers, which are responsible for an interconnected network, capable of efficiently carrying loads.

In general, HDPE has a ductile behavior, and since it is reinforced with lignocellulosic fibers that exhibit a brittle behavior, the respective composites are also brittle [77]. The impact strength of the composites is a measure of the composites' toughness, with the main factors controlling this property being the matrix and fiber properties, as well as matrix–fiber interface [78]. When specimens are subjected to a force, they absorb the energy of the impact, and that energy is dissipated by certain mechanisms, which include fracture, delamination, and fiber pull-outs [79]. The main failure mechanism in the studied composites is fiber pull-outs, since there is not significant interfacial adhesion between the fibers and the matrix. So, as seen in Figure 12d, the introduction of different kinds of fibers in HDPE leads to a gradual decrease in the impact strength, which is in all cases significantly lower than that of neat HDPE. This may be due to the interfaces that act as stress-gathering points, from where cracks may initiate and propagate, and upon increasing filler content,

the number of interfaces becomes high, progressively lowering the composites' overall impact strength.

4. Conclusions

A standardized procedure is proposed in the present study, which will be able to provide comparative estimations of the performance of lignocellulosic-based polymer composites based on a thorough study of individual plant fibers. SEM microphotographs are employed in order to study the fibers' morphology, size, surface roughness, and the existence of any surface-lump materials. Moreover, XRD is employed for the estimation of the crystalline index, which is an indirect way of comparatively estimating the amount of cellulose in each fiber. Furthermore, the TGA of fibers is mostly applied for the comparative estimation of moisture content and for the study of the fibers' behavior at the processing temperature of respective composites, since the integrity of the natural composites is highly dependent on it.

Kenaf demonstrates the highest average fiber diameter, followed by hemp, then ramie, and finally flax, according to the SEM microphotographs. Flax stands out for having the highest lump-material content due to the numerous deposited substances observed on its surface, whereas ramie is notable for its enhanced smoothness, characterized by a uniform and plain texture. For kenaf, its visual appearance appears jagged and irregular due to its fibers primarily consisting of interconnected elementary fibers that form bundles. Correspondingly, hemp displays a partially similar characteristic, with fibers also exhibiting a slightly segmented appearance and surfaces that are less grooved compared to those of kenaf. According to XRD, ramie and kenaf demonstrate higher levels of crystallinity, implying greater cellulose contents, while kenaf possesses the lowest crystallinity index among the compared fibers. Moreover, according to the TGA, ramie has the lowest moisture content, followed by hemp, then flax, and finally kenaf, which has the highest moisture content among the studied fibers. Finally, ramie exhibits the lowest mass loss at the processing temperature of the corresponding composites, followed by hemp, flax, and kenaf, in increasing order of mass loss.

The subsequent study of the respective polymer composites of various filler contents (10, 20, and 30 wt.%) discusses aspects which are affected by the outcomes of the aforementioned characterization techniques. The thermal stability of polymer composites is studied by means of TGA, where composites whose fibers exhibit higher crystallinity indexes and less moisture absorption, namely ramie and hemp, present greater thermal stability. Moreover, the SEM of polymer composites allows for the study of the extent of interfacial adhesion, which at present study is poor for all fiber-based composites, leading to the low wettability of fibers and to impaired mechanical performance, because no chemical modification is performed in the materials, since the crystallinity of fibers should remain intact and with no crystallinity alterations that extra chemical steps could grant. Furthermore, each composite's mechanical performance is multivariate, but it mainly depends on the particle size, volume fraction, filler–matrix adherence, and degree of filler dispersion. Fibers with smaller diameters and greater crystalline indexes, namely ramie–hemp–flax, present greater Young's modulus values of the corresponding composites, while the interplay between the aforementioned factors leads to various trends when referring to the effect of filler content on the strength of composites.

Author Contributions: Conceptualization, D.N.B. and K.C.; methodology D.P., E.P., D.N.B. and K.C.; investigation D.P., E.P., D.N.B. and K.C.; writing—original draft preparation, D.P.; writing—review and editing, D.P., E.P. E.T., D.N.B. and K.C.; supervision, E.P., D.N.B. and K.C. All authors have read and agreed to the published version of the manuscript.

Funding: This research received no external funding.

Institutional Review Board Statement: Not applicable.

Informed Consent Statement: Not applicable.

Data Availability Statement: The raw data supporting the conclusions of this article will be made available by the authors on request.

Conflicts of Interest: The authors declare no conflicts of interest.

References

- Raza, S.; Zhang, J.; Ali, I.; Li, X.; Liu, C. Recent Trends in the Development of Biomass-Based Polymers from Renewable Resources and Their Environmental Applications. *J. Taiwan Inst. Chem. Eng.* **2020**, *115*, 293–303. [[CrossRef](#)]
- Musa, A.A.; Onwualu, A.P. Potential of Lignocellulosic Fiber Reinforced Polymer Composites for Automobile Parts Production: Current Knowledge, Research Needs, and Future Direction. *Heliyon* **2024**, *10*, e24683. [[CrossRef](#)] [[PubMed](#)]
- Roumeli, E.; Terzopoulou, Z.; Pavlidou, E.; Chrissafis, K.; Papadopoulou, E.; Athanasiadou, E.; Triantafyllidis, K.; Bikaris, D. Effect of Maleic Anhydride on the Mechanical and Thermal Properties of Hemp/High-Density Polyethylene Green Composites. *J. Therm. Anal. Calorim.* **2015**, *121*, 93–105. [[CrossRef](#)]
- Xanthopoulou, E.; Chrysafi, I.; Polychronidis, P.; Zamboulis, A.; Bikaris, D.N. Evaluation of Eco-Friendly Hemp-Fiber-Reinforced Recycled HDPE Composites. *J. Compos. Sci.* **2023**, *7*, 138. [[CrossRef](#)]
- Prasad, V.; Alliyankal Vijayakumar, A.; Jose, T.; George, S.C. A Comprehensive Review of Sustainability in Natural-Fiber-Reinforced Polymers. *Sustainability* **2024**, *16*, 1223. [[CrossRef](#)]
- Feng, Y.; Hao, H.; Lu, H.; Chow, C.L.; Lau, D. Exploring the Development and Applications of Sustainable Natural Fiber Composites: A Review from a Nanoscale Perspective. *Compos. B Eng.* **2024**, *276*, 111369. [[CrossRef](#)]
- Kurien, R.A.; Maria Anil, M.; Sharan Mohan, S.L.; Anna Thomas, J. Natural Fiber Composites as Sustainable Resources for Emerging Applications—A Review. *Mater. Today Proc.* **2023**. [[CrossRef](#)]
- Keya, K.N.; Kona, N.A.; Koly, F.A.; Maraz, K.M.; Islam, M.N.; Khan, R.A. Natural Fiber Reinforced Polymer Composites: History, Types, Advantages and Applications. *Mater. Eng. Res.* **2019**, *1*, 69–85. [[CrossRef](#)]
- Shekar, H.S.S.; Ramachandra, M. Green Composites: A Review. *Mater. Today Proc.* **2018**, *5*, 2518–2526. [[CrossRef](#)]
- Asim, M.; Saba, N.; Jawaid, M.; Nasir, M. 12—Potential of Natural Fiber/Biomass Filler-Reinforced Polymer Composites in Aerospace Applications. In *Sustainable Composites for Aerospace Applications*; Jawaid, M., Thariq, M., Eds.; Woodhead Publishing: Cambridge, MA, USA, 2018; pp. 253–268, ISBN 978-0-08-102131-6.
- Rangappa, S.M.; Siengchin, S.; Parameswaranpillai, J.; Jawaid, M.; Ozbakkaloglu, T. Lignocellulosic Fiber Reinforced Composites: Progress, Performance, Properties, Applications, and Future Perspectives. *Polym. Compos.* **2022**, *43*, 645–691. [[CrossRef](#)]
- John, M.; Anandjiwala, R. Recent Developments in Chemical Modification and Characterization of Natural Fiber-reinforced Composites. *Polym. Compos.* **2008**, *29*, 187–207. [[CrossRef](#)]
- Punia Bangar, S.; Ilyas, R.A.; Chaudhary, N.; Dhull, S.B.; Chowdhury, A.; Lorenzo, J.M. Plant-Based Natural Fibers For Food Packaging: A Green Approach To The Reinforcement of Biopolymers. *J. Polym. Environ.* **2023**, *31*, 5029–5049. [[CrossRef](#)]
- Santos, T.F.; Santos, C.M.; Aquino, M.S.; Suyambulingam, I.; Kamil Hussein, E.; Verma, A.; Rangappa, S.M.; Siengchin, S.; Nascimento, J.H.O. Towards Sustainable and Ecofriendly Polymer Composite Materials from Bast Fibers: A Systematic Review. *Eng. Res. Express* **2024**, *6*, 012501. [[CrossRef](#)]
- Siddiqui, S.A.; Yang, X.; Deshmukh, R.K.; Gaikwad, K.K.; Bahmid, N.A.; Castro-Muñoz, R. Recent Advances in Reinforced Bioplastics for Food Packaging—A Critical Review. *Int. J. Biol. Macromol.* **2024**, *263*, 130399. [[CrossRef](#)] [[PubMed](#)]
- Asyraf, M.R.M.; Syamsir, A.; Ishak, M.R.; Sapuan, S.M.; Nurazzi, N.M.; Norrrahim, M.N.F.; Ilyas, R.A.; Khan, T.; Rashid, M.Z.A. Mechanical Properties of Hybrid Lignocellulosic Fiber-Reinforced Biopolymer Green Composites: A Review. *Fibers Polym.* **2023**, *24*, 337–353. [[CrossRef](#)]
- Rahman, M.M.; Maniruzzaman, M.; Yeasmin, M.S. A State-of-the-Art Review Focusing on the Significant Techniques for Naturally Available Fibers as Reinforcement in Sustainable Bio-Composites: Extraction, Processing, Purification, Modification, as Well as Characterization Study. *Results Eng.* **2023**, *20*, 101511. [[CrossRef](#)]
- Parameswaranpillai, J.; Gopi, J.A.; Radoor, S.; Krishnasamy, S.; Deshmukh, K.; Hameed, N.; Salim, N.V.; Sienkiewicz, N. Turning Waste Plant Fibers into Advanced Plant Fiber Reinforced Polymer Composites: A Comprehensive Review. *Compos. Part C Open Access* **2023**, *10*, 100333. [[CrossRef](#)]
- Rana, A.K.; Singha, A.S.; Kumari, M.; Kumar, V. Effect of Chemical Functionalization on Functional Properties of Cellulosic Fiber-Reinforced Polymer Composites. In *Lignocellulosic Polymer Composites*; Wiley Online Library: Hoboken, NJ, USA, 2014; pp. 281–299.
- Thakur, M.K.; Rana, A.K.; Thakur, V.K. Lignocellulosic Polymer Composites: A Brief Overview. In *Lignocellulosic Polymer Composites: Processing, Characterization, and Properties*; Wiley Online Library: Hoboken, NJ, USA, 2015; pp. 1–15, ISBN 9781118773949.
- Dittenber, D.B.; GangaRao, H.V.S. Critical Review of Recent Publications on Use of Natural Composites in Infrastructure. *Compos. Part. A* **2012**, *43*, 1419–1429. [[CrossRef](#)]
- Chakkour, M.; Ould Moussa, M.; Khay, I.; Balli, M.; Ben Zineb, T. Towards Widespread Properties of Cellulosic Fibers Composites: A Comprehensive Review. *J. Reinf. Plast. Compos.* **2022**, *42*, 222–263. [[CrossRef](#)]
- Thapliyal, D.; Verma, S.; Sen, P.; Kumar, R.; Thakur, A.; Tiwari, A.K.; Singh, D.; Verros, G.D.; Arya, R.K. Natural Fibers Composites: Origin, Importance, Consumption Pattern, and Challenges. *J. Compos. Sci.* **2023**, *7*, 506. [[CrossRef](#)]
- Meshram, J. Biology of Industrial Bast Fibers with Reference to Quality. *J. Nat. Fibers* **2013**, *10*, 176–196. [[CrossRef](#)]

25. Manral, A.; Bajpai, P.K. Analysis of Natural Fiber Constituents: A Review. *IOP Conf. Ser. Mater. Sci. Eng.* **2018**, *455*, 012115. [[CrossRef](#)]
26. Mohammed, M.; Olewi, J.K.; Mohammed, A.M.; Jawad, A.J.M.; Osman, A.F.; Adam, T.; Betar, B.O.; Gopinath, S.C.B.; Dahham, O.S.; Jaafar, M. Comprehensive Insights on Mechanical Attributes of Natural-Synthetic Fibres in Polymer Composites. *J. Mater. Res. Technol.* **2023**, *25*, 4960–4988. [[CrossRef](#)]
27. Akil, H.M.; Omar, M.F.; Mazuki, A.A.M.; Safiee, S.; Ishak, Z.A.M.; Abu Bakar, A. Kenaf Fiber Reinforced Composites: A Review. *Mater. Des.* **2011**, *32*, 4107–4121. [[CrossRef](#)]
28. Tumuluru, J.S.; Sokhansanj, S.; Hess, J.; Wright, C.; Boardman, R. A Review on Biomass Torrefaction Process and Product Properties for Energy Applications. *Ind. Biotechnol.* **2011**, *7*, 384–401. [[CrossRef](#)]
29. Prasanth, R.; Shankar, R.; Dilfi, A.; Thakur, V.K.; Ahn, J.-H. Eco-Friendly Fiber-Reinforced Natural Rubber Green Composites: A Perspective on the Future. In *Green Composites from Natural Resources*; Thakur, V.K., Ed.; CRC Press: Boca Raton, FL, USA, 2013; pp. 205–254.
30. Thakur, V.K.; Sinha, A.S. *Biomass-Based Biocomposites*; Smithers Rapra: Shropshire, UK, 2013; ISBN 1847359809/9781847359803/1847359817/9781847359810.
31. Thakur, V.K.; Thakur, M.K.; Gupta, R.K.; Prasanth, R.; Michael, R. Kessler Green Composites: An Introduction. In *Green Composites from Natural Resources*; Thakur, V.K., Ed.; CRC Press: Boca Raton, FL, USA, 2013; pp. 1–10.
32. Djafari Petroudy, S.R. 3—Physical and Mechanical Properties of Natural Fibers. In *Advanced High Strength Natural Fibre Composites in Construction*; Fan, M., Fu, F., Eds.; Woodhead Publishing: Cambridge, MA, USA, 2017; pp. 59–83, ISBN 978-0-08-100411-1.
33. Bismarck, A.; Mishra, S.; Lampke, T. Plant Fibers as Reinforcement for Green Composites. In *Natural Fibers, Biopolymers, and Biocomposites*; Taylor and Francis: Abingdon, UK, 2005; pp. 37–108, ISBN 0203508203.
34. Aziz, S.H.; Ansell, M.P. Optimising the Properties of Green Composites. In *Green Composites: Polymer Composites and the Environment*; Baillie, C., Ed.; Woodhead Publishing Ltd.: Cambridge, MA, USA, 2004; pp. 154–180, ISBN 9781855737396.
35. Olesen, P.; Plackett, D. Perspectives on the performance of natural plant fibres. In Proceedings of the International Conference Natural Fibres Performance Forum, Copenhagen, Denmark, 27–28 May 1999.
36. Carrier, M.; Loppinet-Serani, A.; Denux, D.; Lasnier, J.-M.; Ham-Pichavant, F.; Cansell, F.; Aymonier, C. Thermogravimetric Analysis as a New Method to Determine the Lignocellulosic Composition of Biomass. *Biomass Bioenergy* **2013**, *35*, 298–307. [[CrossRef](#)]
37. Borysiak, S.; Doczekalska, B. X-ray Diffraction Study of Pine Wood Treated with NaOH. *Fibres Text. East. Eur.* **2005**, *13*, 87–89.
38. Mohanty, A.K.; Misra, M.; Hinrichsen, G. Biofibres, Biodegradable Polymers and Biocomposites: An Overview. *Macromol. Mater. Eng.* **2000**, *276–277*, 1–24. [[CrossRef](#)]
39. Barbero, E.J. *Introduction to Composite Materials Design*; CRC Press: Boca Raton, FL, USA, 1999; ISBN 9781560327011.
40. Indran, S.; Raj, R.E. Characterization of New Natural Cellulosic Fiber from Cissus Quadrangularis Stem. *Carbohydr. Polym.* **2015**, *117*, 392–399. [[CrossRef](#)]
41. Bledzki, A.K.; Reihmane, S.; Gassan, J. Properties and Modification Methods for Vegetable Fibers for Natural Fiber Composites. *J. Appl. Polym. Sci.* **1996**, *59*, 1329–1336. [[CrossRef](#)]
42. Fowler, P.A.; Hughes, J.M.; Elias, R.M. Biocomposites: Technology, Environmental Credentials and Market Forces. *J. Sci. Food Agric.* **2006**, *86*, 1781–1789. [[CrossRef](#)]
43. Satyanarayana, K.G.; Arizaga, G.G.C.; Wypych, F. Biodegradable Composites Based on Lignocellulosic Fibres—An Overview. *Prog. Polym. Sci.* **2009**, *34*, 982–1021. [[CrossRef](#)]
44. Kandimalla, R.; Kalita, S.; Choudhury, B.; Devi, D.; Kalita, D.; Kalita, K.; Dash, S.; Kotoky, J. Fiber from Ramie Plant (*Boehmeria Nivea*): A Novel Suture Biomaterial. *Mater. Sci. Eng. C* **2016**, *62*, 816–822. [[CrossRef](#)] [[PubMed](#)]
45. Ahvenainen, P.; Kontro, I.; Svedström, K. Comparison of Sample Crystallinity Determination Methods by X-Ray Diffraction for Challenging Cellulose I Materials. *Cellulose* **2016**, *23*, 1073–1086. [[CrossRef](#)]
46. ASTM D638-22; Standard Test Method for Tensile Properties of Plastics. ASTM—American Society for Testing and Material: West Conshohocken, PA, USA, 2022.
47. ASTM D256-23; Standard Test Methods for Determining the Izod Pendulum Impact Resistance of Plastics. ASTM—American Society for Testing and Material: West Conshohocken, PA, USA, 2023.
48. Zhang, K.; Wang, F.; Liang, W.; Wang, Z.; Duan, Z.; Yang, B. Thermal and Mechanical Properties of Bamboo Fiber Reinforced Epoxy Composites. *Polymers* **2018**, *10*, 608. [[CrossRef](#)] [[PubMed](#)]
49. Poletto, M.; Zeni, M.; Zattera, A.J. Effects of Wood Flour Addition and Coupling Agent Content on Mechanical Properties of Recycled Polystyrene/Wood Flour Composites. *J. Thermoplast. Compos. Mater.* **2011**, *25*, 821–833. [[CrossRef](#)]
50. Monteiro, S.N.; Lopes, F.P.D.; Barbosa, A.P.; Bevitori, A.B.; Da Silva, I.L.A.; Da Costa, L.L. Natural Lignocellulosic Fibers as Engineering Materials—An Overview. *Metall. Mater. Trans. A* **2011**, *42*, 2963. [[CrossRef](#)]
51. Monteiro, S.N.; Satyanarayana, K.G.; Ferreira, A.S.; Nascimento, D.C.O.; Lopes, F.P.D.; Silva, I.L.A.; Bevitori, A.B.; Inácio, W.P.; Bravo Neto, J.; Portela, T.G. Selection of High Strength Natural Fibers. *Matéria* **2010**, *15*, 488–505. [[CrossRef](#)]
52. Bledzki, A.K.; Mamun, A.A.; Volk, J. Physical, Chemical and Surface Properties of Wheat Husk, Rye Husk and Soft Wood and Their Polypropylene Composites. *Compos. Part A Appl. Sci. Manuf.* **2010**, *41*, 480–488. [[CrossRef](#)]
53. Patil, N.V.; Rahman, M.M.; Netravali, A.N. “Green” Composites Using Bioresins from Agro-Wastes and Modified Sisal Fibers. *Polym. Compos.* **2019**, *40*, 99–108. [[CrossRef](#)]

54. Popescu, M.-C.; Popescu, C.-M.; Lisa, G.; Sakata, Y. Evaluation of Morphological and Chemical Aspects of Different Wood Species by Spectroscopy and Thermal Methods. *J. Mol. Struct.* **2011**, *988*, 65–72. [[CrossRef](#)]
55. John, M.J.; Thomas, S. Biofibres and Biocomposites. *Carbohydr. Polym.* **2008**, *71*, 343–364. [[CrossRef](#)]
56. Gümüşkaya, E.; Usta, M.; Kirci, H. The Effects of Various Pulping Conditions on Crystalline Structure of Cellulose in Cotton Linters. *Polym. Degrad. Stab.* **2003**, *81*, 559–564. [[CrossRef](#)]
57. French, A.D. Idealized Powder Diffraction Patterns for Cellulose Polymor1. *Cellulose* **2014**, *21*, 885–896. [[CrossRef](#)]
58. Segal, L.; Creely, J.J.; Martin, A.E.; Conrad, C.M. An Empirical Method for Estimating the Degree of Crystallinity of Native Cellulose Using the X-Ray Diffractometer. *Text. Res. J.* **1959**, *29*, 786–794. [[CrossRef](#)]
59. Bansal, P.; Hall, M.; Realff, M.J.; Lee, J.H.; Bommaris, A.S. Multivariate Statistical Analysis of X-Ray Data from Cellulose: A New Method to Determine Degree of Crystallinity and Predict Hydrolysis Rates. *Bioresour. Technol.* **2010**, *101*, 4461–4471. [[CrossRef](#)] [[PubMed](#)]
60. Park, S.; Baker, J.O.; Himmel, M.E.; Parilla, P.A.; Johnson, D.K. Cellulose Crystallinity Index: Measurement Techniques and Their Impact on Interpreting Cellulase Performance. *Biotechnol. Biofuels* **2010**, *3*, 10. [[CrossRef](#)] [[PubMed](#)]
61. Terinte, N.; Ibbett, R.N.; Schuster, K.C. Overview on Native Cellulose and Microcrystalline Cellulose I Structure Studied by X-Ray Diffraction (WAXD): Comparison between Measurement Techniques. *Lenzing. Berichte* **2011**, *89*, 118–131.
62. Ferro, M.; Mannu, A.; Panzeri, W.; Theeuwen, C.H.J.; Mele, A. An Integrated Approach to Optimizing Cellulose Mercerization. *Polymers* **2020**, *12*, 1559. [[CrossRef](#)]
63. Tajvidi, M.; Takemura, A. Thermal Degradation of Natural Fiber-Reinforced Polypropylene Composites. *J. Thermoplast. Compos. Mater.* **2010**, *23*, 281–298. [[CrossRef](#)]
64. Rachini, A.; Le Troedec, M.; Peyratout, C.; Smith, A. Comparison of the Thermal Degradation of Natural, Alkali-Treated and Silane-Treated Hemp Fibers under Air and an Inert Atmosphere. *J. Appl. Polym. Sci.* **2009**, *112*, 226–234. [[CrossRef](#)]
65. Bismarck, A.; Mohanty, A.; Aranberri, I.; Czapla, S.; Misra, M.; Hinrichsen, G.; Springer, J. Surface Characterization of Natural Fibers; Surface Properties and the Water up-Take Behavior of Modified Sisal and Coir Fibers. *Green Chem.* **2001**, *3*, 100–107. [[CrossRef](#)]
66. Papadopoulou, E.; Chrysafi, I.; Karidi, K.; Mitani, A.; Bikaris, D.N. Particleboards with Recycled Material from Hemp-Based Panels. *Materials* **2024**, *17*, 139. [[CrossRef](#)] [[PubMed](#)]
67. Varma, D.S.; Varma, M.; Varma, I.K. Thermal Behaviour of Coir Fibres. *Thermochim. Acta* **1986**, *108*, 199–210. [[CrossRef](#)]
68. Yang, H.; Yan, R.; Chen, H.; Lee, D.H.; Zheng, C. Characteristics of Hemicellulose, Cellulose and Lignin Pyrolysis. *Fuel* **2007**, *86*, 1781–1788. [[CrossRef](#)]
69. Neto, J.S.S.; de Queiroz, H.F.M.; Aguiar, R.A.A.; Banea, M.D. A Review on the Thermal Characterisation of Natural and Hybrid Fiber Composites. *Polymers* **2021**, *13*, 4425. [[CrossRef](#)]
70. Banik, N.; Dey, V.; Sastry, G.R.K. An Overview of Lignin & Hemicellulose Effect Upon Biodegradable Bamboo Fiber Composites Due to Moisture. *Mater. Today Proc.* **2017**, *4*, 3222–3232. [[CrossRef](#)]
71. Thomason, J.L.; Rudeiros-Fernández, J.L. Thermal Degradation Behaviour of Natural Fibres at Thermoplastic Composite Processing Temperatures. *Polym. Degrad. Stab.* **2021**, *188*, 109594. [[CrossRef](#)]
72. Chen, Z.; Hu, M.; Zhu, X.; Guo, D.; Liu, S.; Hu, Z.; Xiao, B.; Wang, J.; Laghari, M. Characteristics and Kinetic Study on Pyrolysis of Five Lignocellulosic Biomass via Thermogravimetric Analysis. *Bioresour. Technol.* **2015**, *192*, 441–450. [[CrossRef](#)]
73. Purnama, P.; Kim, S.H. Biodegradable Blends of Stereocomplex Polylactide and Lignin by Supercritical Carbon Dioxide-Solvent System. *Macromol. Res.* **2014**, *22*, 74–78. [[CrossRef](#)]
74. Shebani, A.; Van Reenen, A.; Meincken, M. The Effect of Wood Species on the Mechanical and Thermal Properties of Wood–LLDPE Composites. *J. Compos. Mater.* **2009**, *43*, 1305–1318. [[CrossRef](#)]
75. Fu, S.-Y.; Feng, X.-Q.; Lauke, B.; Mai, Y.-W. Effects of Particle Size, Particle/Matrix Interface Adhesion and Particle Loading on Mechanical Properties of Particulate–Polymer Composites. *Compos. B Eng.* **2008**, *39*, 933–961. [[CrossRef](#)]
76. Švab, I.; Musil, V.; Leskovac, M. The Adhesion Phenomena in Polypropylene/Wollastonite Composites. *Acta Chim. Slov.* **2005**, *52*, 264–271.
77. Shahzad, A. 11—Mechanical Properties of Lignocellulosic Fiber Composites. In *Lignocellulosic Fibre and Biomass-Based Composite Materials*; Jawaid, M., Md Tahir, P., Saba, N., Eds.; Woodhead Publishing Series in Composites Science and Engineering; Woodhead Publishing: Cambridge, MA, USA, 2017; pp. 193–223, ISBN 978-0-08-100959-8.
78. NagarajaGanesh, B.; Rekha, B. Morphology and Damage Mechanism of Lignocellulosic Fruit Fibers Reinforced Polymer Composites: A Comparative Study. *SN Appl. Sci.* **2019**, *1*, 1250. [[CrossRef](#)]
79. NagarajaGanesh, B.; Muralikannan, R. Physico-Chemical, Thermal, and Flexural Characterization of Cocos Nucifera Fibers. *Int. J. Polym. Anal. Charact.* **2016**, *21*, 244–250. [[CrossRef](#)]

Disclaimer/Publisher’s Note: The statements, opinions and data contained in all publications are solely those of the individual author(s) and contributor(s) and not of MDPI and/or the editor(s). MDPI and/or the editor(s) disclaim responsibility for any injury to people or property resulting from any ideas, methods, instructions or products referred to in the content.